Electronic Journal of Structural Engineering

Original Article

Cite this:
DOI:https://doi.org/10.56748/ejse.234433

Received Date: 14 April 2023
Accepted Date: 16 June 2023

1443-9255
https://ejsei.com/ejse

Dynamic response analysis of the process of the utility shield tunnel under-passing the operating subway tunnel.

Jing Sun [a], Xingkai Pei [a], Cheng Yang [a] and Binzhong Zhu[b]*
[a] Guangzhou Metro Design & Research Institute Co., Ltd. Guangzhou, China
[b] Southwest Jiaotong University, Chengdu, China
* Corresponding Author: 942194008@qq.com

Abstract

To analyze the interaction between the operating subway tunnel and the utility tunnel under construction during the utility tunnel under-passing the subway tunnel, an operating tunnel-stratum-utility shield tunnel coupled dynamic calculation model is established taking the utility tunnel under construction under-passing the Guangzhou-Foshan line subway project as an example. And the interaction between the existing tunnel and utility tunnel was studied. The results show that the amplitude change of the vertical displacement, acceleration and additional vertical stress are most influenced by the under-passing shield tunnel when the train operating on one line, and the max changes are 0.01mm, 0.03m/s^2 and 1.5kPa, respectively. The vertical displacement and acceleration response generated by the train operation during the excavation of the new tunnel can be neglected, but the vertical additional stress will have the max change of 2.1kPa. The closer the distance between the train load to the new and old tunnel structures are, the greater the displacement, acceleration and additional stresses of the new and old tunnel structures are when the trains are running in different lines. Structural safety calculations show that the old and new tunnel structures are safe during the utility shield tunnel under-passing. The study can provide useful reference for the construction and operation of similar tunnels.

Keywords

The utility shield tunnel, Operating subway tunnel, Dynamic train load, Dynamic response

1. Introduction

With the rapid development of urban underground space in China, the underground traffic network and municipal pipeline laying are becoming more and more complex, and some tunnels under construction inevitably appear to cross and overlap with existing tunnels. The surrounding soil, the lining structures and train tracks of existing tunnels which are crossed or overlapped will be deformed or damaged by the influence of the construction of new tunnels, and the safety of subway traffic will be endangering (Luo et al, 2014; Bo et al, 2014; Li et al, 2014). The existing tunnels, especially the operating subway will generate large dynamic stresses in the foundation under the cyclic train loads, which will adversely affect both the operating tunnel itself and the excavation of the tunnel under construction (Zhang et al, 2021; Huang et al, 2021; Gharehdash et al, 2015).

Currently, the dynamic effects of train loads on tunnel structures are receiving more and more attention from scholars. Saba Gharehdash and Milad Barzegar (2015) studied the dynamic response of the shield tunnel lining and its soft ground foundation under the cycle train load by establishing an elastic-plastic 3D finite difference model considering lining joints, found that the dynamic response of the structure near the joints and the foundation soil under the shield tunnel segment was more intense. Yan et al (2018) used nonlinear finite element software to capture the tensile, shear and bending behaviors of shield tunnel lining under train vibration load, revealing the vibration response characteristics of the tunnel structure under the train vibration load. Yang et al (2022) studied the dynamic response of the shield tunnel segment and its internal structure and the attenuation characteristics of vibration waves at the subgrade based on time-frequency analysis by the model tests and numerical simulations, found that the dynamic response of the tunnel lining increased with frequency in the full frequency domain under train loading, and the train displacement effect increased the dynamic response of the tunnel structure. Tian et al (2021) studied the dynamic response and the fatigue damage of the tunnel structure by establishing a 3D model considering the initial defects of shield tunnel structure, and found that the higher the train speed is, the longer the final cracks of lining are, and the train axle weight has a greater effect on the tube sheet crack length than the train speed. Train loads are cyclic loads, and many scholars have predicted tunnel life based on Miner's linear cumulative damage theory or other improved damage theories (Xu et al, 2020; Liu et al, 2016; Wang et al, 2017).

The above studies have made many advances on the vibration characteristics, damage behavior and fatigue life of tunnel structures under train load. But the dynamic response and damage of the operating tunnel due to tunnel adjacent construction was not involved. Liu et al (2013) paid attention to the effect of train load on sensitive adjacent structures and analyzed the dynamic response of adjacent structures under train load. While many scholars at home and abroad focus more on the stress and deformation of the existing structure, surrounding rock or ground surface due to adjacent construction of tunnel within the scope of static mechanics, less consideration is given to the influence of the train or other traffic loads in operating tunnels on the adjacent structures and surrounding rock (Jin et al, 2019). Lin (2016) studied the dynamic response of the overlapping tunnel structures before, after construction and during the operation phase under train load. Yan et al (2018; 2017) studied the dynamic response of the vertical overlapping tunnels when trains were traveling in the upper tunnels. But the above studies focused on the dynamic characteristics of the tunnel structure under different load combinations and the dynamic response of the operational overlapping tunnels, the dynamic response considers the interaction between the operational tunnel and the adjacent tunnel under construction did not study.

Therefore, it is important to study the interaction between the operating subway tunnel and the tunnel under construction when the new tunnel under pass the operating tunnel to ensure the normal operation of the existing tunnel and the safe construction of new tunnel. In this paper, the dynamic calculation model including the operating tunnel-stratum-utility tunnel under construction is established taking the Guangzhou-Foshan line subway section as example, and the interaction between the existing tunnel and utility tunnel under construction was studied. The research results can provide important references for the construction and operation of similar projects.

Project Summary

The main line of the utility tunnel in the central city of Guangzhou is 44.9km long, and the construction is mainly based on the shield method. The utility tunnel is a closed loop around the central city, so its line has to cross with the operating or under-construction subway lines many times, including the first subway cross-prefecture-level administrative district -- Guangzhou-Foshan line (crossing with operating tunnel at Yangang-Shixi section), as shown in fig.1a. The utility tunnel crossing the Guang-Fo Line section is 15.2m deep, with a minimum clear distance of only 2.37m (as shown in fig.1b), which has a high safety risk for construction.

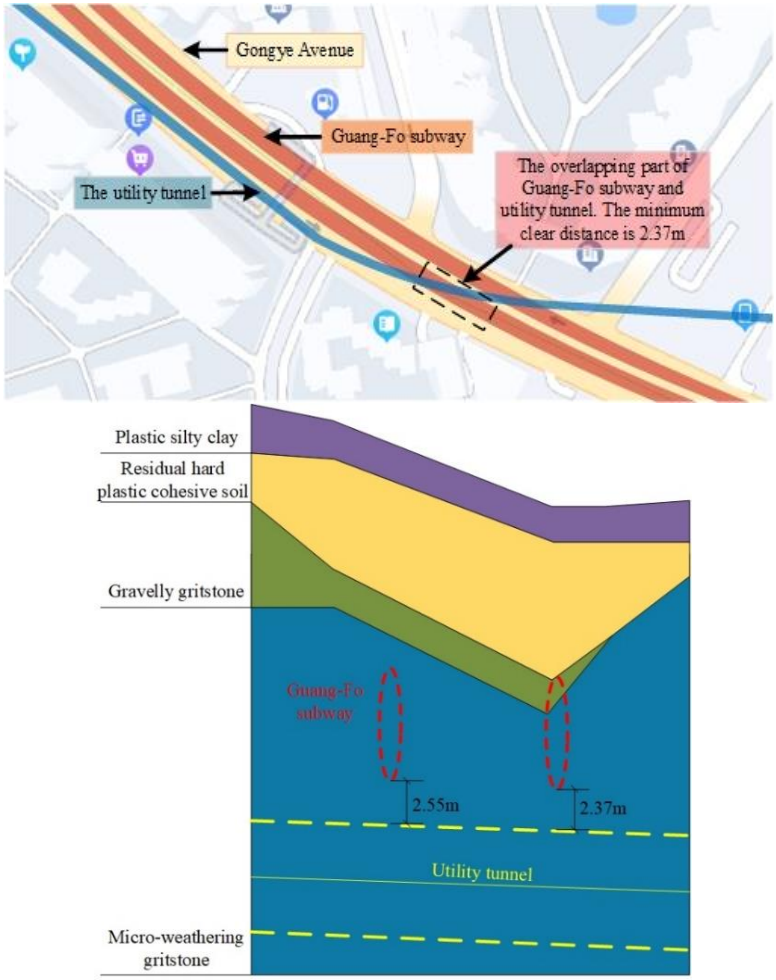

Fig.1 The schematic diagram and geological section overlapping of Guang-Fo Metro and the Utility tunnel.

Table 1. Physical and mechanical parameters of the soil layer.

Material name	Density (kg/m³)	Elastic modulus (MPa)	Poisson ratio	Friction angle (°)	Cohesion (MPa)
Plastic silty clay	19.6	15	0.28	12	18
Residual hard plastic cohesive soil	19.6	28	0.26	18.4	26
Gravelly gritstone	22.2	70	0.24	26	30
Micro-weathering gritstone	25.9	1500	0.20	29	750

The inner and outer diameters of the lining of the utility tunnel under-passing the operating subway tunnel section is 5.4mm and 6.0mm respectively, each ring is 1.2m longitudinally. The Guang-Fo Line is also a shield tunnel, and the inner and outer diameters of the lining are consistent with the utility tunnel. The soil underneath the site is complex, mainly including plastic silty clay, residual hard plastic cohesive soil, gravelly gritstone and micro-weathering gritstone. The operating tunnels mainly cross the gravelly gritstone and micro-weathering gritstone, while the utility tunnel is all located in the micro-weathering gritstone. The physical and mechanical parameters of the soils in the site investigation report are shown in Table 1.

Construction safety is ensured during construction by the following measures: 1) automated monitoring before and after crossing the operating tunnel; 2) setting up test sections to determine crossing parameters of TBM; 3) controlling the advance speed and jacking force of the TBM based on automated monitoring data and feedback information to strengthen synchronous grouting. Strengthen secondary grouting after shield crossing.

2. NUMERICAL MODELS

2.1 Model building

In this study, the stratums above and below the intersection section of the utility tunnel and the operating subway tunnel are simplified to a homogeneous stratum, and a 3D model with dimensions of 130m × 90m × 50m (length × width × height) is established according to the requirements of Saint Venant's Principle and computational accuracy, as shown in fig.2a. The tunnel lining is C50 reinforced concrete with a thickness of 0.3 m. Considering that the dynamic analysis takes up many computational resources, the effect of shield tunnel joints is ignored and the model flexural stiffness is appropriately discounted according to the equivalent flexural stiffness formula (1) (Yan et al, 2010) (the result of the tunnel lining flexural stiffness discount is 4.6×10^7kN • m²) to simulate the effect of joints.

$$(EI)_{\text{eq}} = \frac{\cos^3\varphi}{\cos\varphi + \left(\frac{\pi}{2}+\varphi\right)} E_s I_s$$
$$\varphi + \cot\varphi = \pi\left(0.5 + \frac{K_j}{\frac{E_s A_s}{l_s}}\right) \quad (1)$$

Where φ is the angle between the neutral axis and the horizontal line of the tunnel center; E_s is the elastic modulus of the lining; I_s is the moment of inertia of the circular section, $I_s = \pi(D^2\text{-}d^2)/64$, where D and dare outer and inner diameter of the tunnel lining; A_s the area of the liner circle; K_j is the single bolt tension stiffness ($K_j = 4.0\times10^5$ in this section); l_s is the width of the lining segment.

In this model, the stratum, tunnel lining, roadbed, sleepers and tracks are simulated by solid unit, and the shield shell and grouting layer are simulated by shell unit with thickness of 0.1m. The constitutive model of the stratum, lining and bed is Mohr-Coulomb model, the sleepers and tracks are elastic model, and the fasteners (as in fig.2b) are simulated by elastic units with a stiffness of 100 kN/mm and a density of 2500 kg/m³ and a damping of 7.0×10^4 N • s/m is added to the fasteners using local damping (Shi, 2020). The stratigraphic parameters were taken according to the site survey report (see Table 1), and the tunnel lining, roadbed, tracks and grouting layer parameters are shown in Table 2.

Table 2 Physical and mechanical parameters of the tunnel structure.

Material name	Density (kg/m³)	Elastic modulus (GPa)	Poisson ratio
C50 shield tunnel segment	25.0	34.5	0.17
Rail-bed	23.0	28.0	0.20
Rail	78.5	210.0	0.30
Grouting layer	20.0	10.5	0.25

To study the interaction between the utility tunnel and the operational tunnel during the adjacent tunnel construction, three locations were taken for the analysis as shown in fig.2c. During the calculation, the monitoring points are located at the top of the latest ring of lining segment (A_1, A_2, A_3) and at the bottom of the arch (B, C) where the operational tunnel crosses the utility tunnel, as shown in fig.2d.

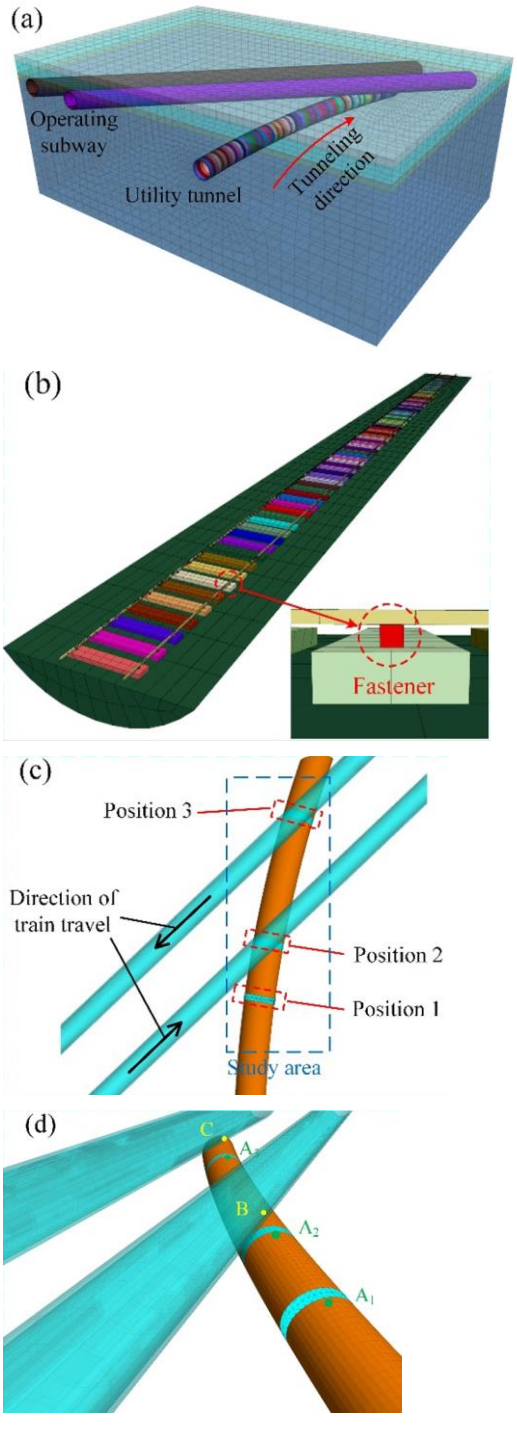

Fig. 2 The numerical model and layout of the monitoring point.

2.2 Materials damping

Rayleigh damping is used in the dynamic calculation process, whose damping matrix is proportional to the mass matrix and stiffness matrix:

$$[C] = \alpha[M] + \beta[K] \tag{2}$$

where $[M]$ and $[K]$ are the mass matrix and stiffness matrix, respectively; $[C]$ is the damping matrix; α and β are the mass damping coefficients and stiffness damping coefficients, whose values are taken with reference to the study of Yan et al. (2018) and are 0.279 and 0.009, respectively.

2.3 Train-induced vibration loads

The vibration load is a single-valued function of time, i.e., $P = P(t)$. Research at the Derby Railway Technology Centre, UK, indicates that train loads are mainly controlled by the smoothness of track, dynamic surcharge loads and waveform wear (Jenkins et al, 1974; Liang et al, 1999), which can be simulated by an excitation function as follows:

$$P(t) = p_0 + p_1 \sin(\omega_1 t) + p_2 \sin(\omega_2 t) + p_3 \sin(\omega_3 t) \tag{3}$$

where p_0 is the train wheel pair static load; p_i (i=1, 2, 3) is the vibration load amplitude, and its expression is

$$p_i = m_0 \alpha_i \omega_i^2 \tag{4}$$

where m_0 is the unspring mass; α_i is the typical vector height under the corresponding control condition; ω_i is the circular frequency of the wavelength of uneven vibration under the corresponding control condition, which is calculated as

$$\omega_i = \frac{2\pi v}{l_i} \tag{5}$$

Where v is the train operating speed; l_i is the typical wavelength under the corresponding control conditions. Considering the train of Guang-Fo line is a B-type train with Tc-M-M_1-T_c total 4-car formation, the length of M and M_1 cars are 19.00m, the length of T_c cars is 19.57m, the axle weight of the train is 14t, the standard gauge of 1435mm is used, and the design max operating speed is 80km/h. According to the axle weight of B-type train and the literature (Yan et al, 2018), this paper takes the unspring mass of B-type train m0=750kg, typical vector height α_1=3.50mm, α_2=0.4mm, α_3=0.08mm, typical wavelength l_1=10.0m, l_2=2.0m, l_3=0.5m. Fig.3 shows the time curve of train vibration load.

When a train is moving along the track, the actual train load should move along the track too. The relation between train position and time is x=v t. In this study, the train load acts on the tracks node and moves longitudinally along the tracks at a speed of 80 km/h by secondary development of FISH language.

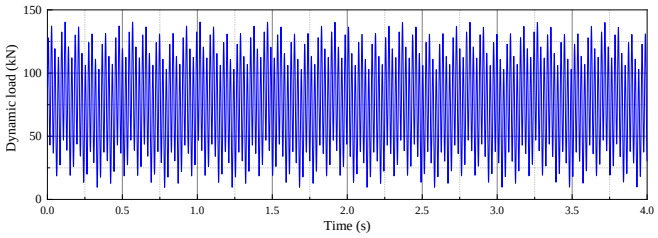

Fig. 3 Vertical vibration load curve of the train (80km/h)

3. Result Analysis

3.1 Influence of the location of the pipe gallery excavation

Comparing the dynamic response of the tunnel structures during train operation before and after the utility tunnel under passing the operating tunnel at the three locations shown in Figure 2c, the interaction between the utility tunnel and operating tunnel is analyzed, with the subway train operating in the right line only.

3.1.1 Displacement response characteristics of tunnel structures

To describe the displacement response of the tunnel structures during train operation, the displacement time curves of each monitoring point when the utility tunnel under pass to different positions and the vertical displacement clouds of the tunnel structures when the vertical displacement reaches its peak (time of about t=5.6s) are presented in fig.4 and fig.5, respectively.

As shown in fig.4, when the utility tunnel excavated to different positions, the displacement response time curve of the tunnel structure is basically the same: when the train approaches the monitoring point, the vertical displacement of the monitoring points gradually increased, and when the train leaves the monitoring point, the vertical displacement of the monitoring points gradually recovered. The measurement points A_1~A_3 on the new tunnel reach the peak vertical displacement first, followed by monitoring point B and monitoring point C. As can be seen from fig.4d, when the utility tunnel under pass to different positions, the peak vertical displacement of each monitoring point shows that the settlement of monitoring point B is the largest, followed by C, and A1~A3 is the smallest. In addition, with the utility tunnel excavation, the displacement extremes of the operating tunnel structures are basically the same, and only the displacement extremes of the utility tunnel structures increase. The excavation position has a certain influence on the vertical displacement extremes of the utility tunnel but has little influence on the vertical displacement extremes of the operating tunnel.

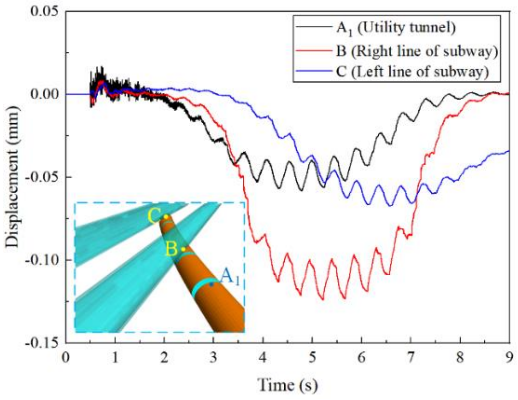

(a)

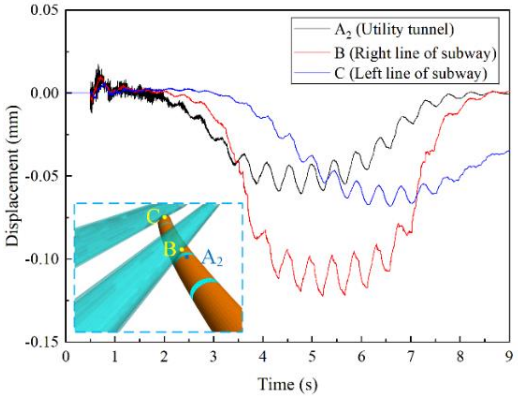

(b)

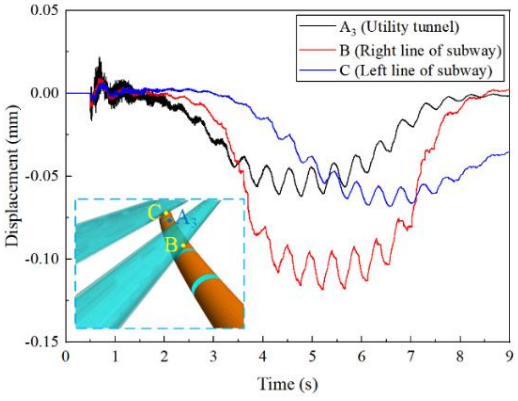

(c)

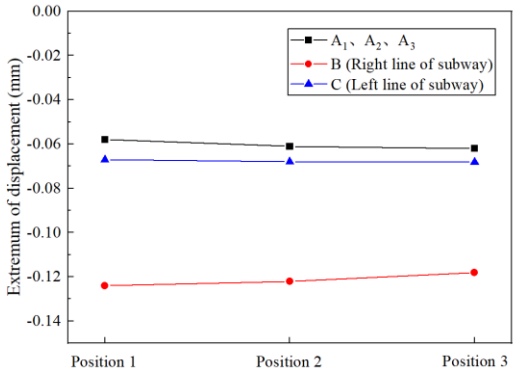

(d)

Fig.4 Dynamic responses of the vertical displacement for the tunnels. a Position 1. b Position 2. c Position 3. d Extremum of displacement in different position.

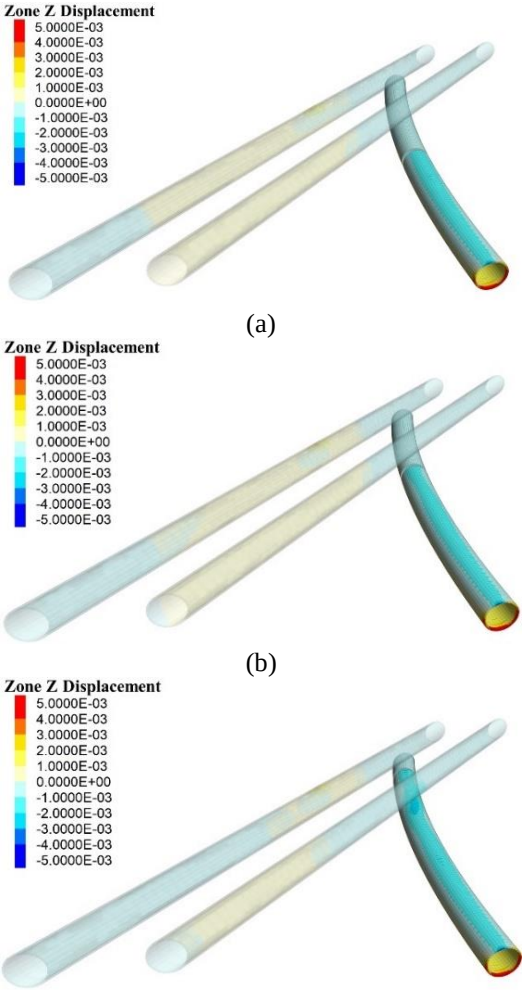

(a)

(b)

(c)

Fig. 5 Vertical displacement contour of the tunnels. a Position 1. b Position 2. c Position 3. (Unit: m)

As can be seen from fig.5, the settlement of the arch of the utility tunnel structure is more obvious with a vertical displacement of 2mm when the utility tunnel is excavated to position 1 and 2. The settlement at the arch of the utility tunnel structure at the intersection position of the utility tunnel and the operating tunnel is the largest with a vertical displacement of to 3mm when the utility tunnel excavated to position 3. It can be seen that the structures on the overlapping intersection position of the utility tunnel and the operating tunnel is the most dangerous while the utility under passed the operating tunnel. When the utility tunnel excavated to different positions, there is a significant difference of vertical displacement in the operating tunnel right line: the settlement of the tunnel structure in front of this significant difference position is about 2mm, while the settlement of other area is about 0. The position of this significant difference appears to move to the rear of the

train travel direction with the excavation of the utility tunnel. This phenomenon is the result of the disturbance from the surrounding soil by the combined action of the utility tunnel construction and the train load.

3.1.2 Operating tunnel structural dynamic response characteristics

From the displacement analysis, the dynamic response of the right line of the operating tunnel is larger than the left line under the train load. To ignore the influence of boundary effects, only the acceleration and vertical additional stress time curves of monitoring point B of train operation are extracted after 3s as shown in fig.6 and fig.7, respectively.

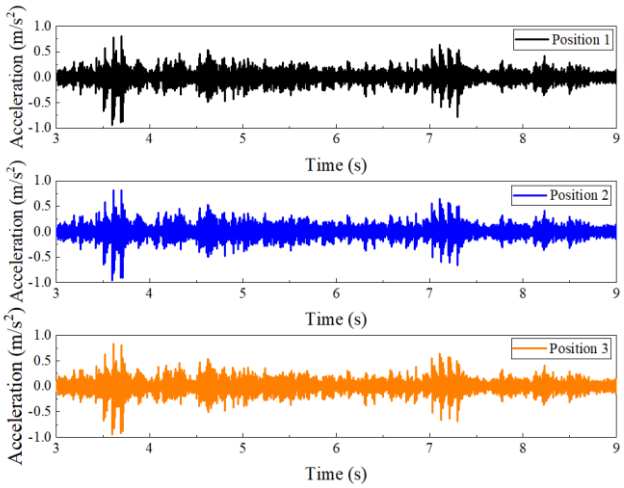

Fig. 6 Dynamic responses of the acceleration for the right line of operating tunnel.

As can be seen from fig.6, the acceleration amplitude at monitoring point B shows a trend of increasing and then decreasing with time. The acceleration amplitude is the largest when the train load is all acted on the model, followed by the second when the train leaves the track, and the max value of acceleration amplitude is smaller than the above two time periods and larger than the other time periods when the train travels through monitoring point B. In addition, the max value of acceleration amplitude of monitoring point B is 0.94m/s², 0.97m/s² and 0.95m/s² when the utility tunnel excavated to different positions. The acceleration amplitude of monitoring point B is the largest when the utility tunnel excavated to position 2. But in general, the acceleration of the operating tunnel structure is less affected by the position of the utility tunnel excavation under the train load. As mentioned above, the train vibration load is affected by the smoothness of track. Combined with Figure 5, the vibration acceleration is not much different because the settlement of the operating tunnel affected by the excavation of the utility tunnel is small. It also shows the reliability of the utility tunnel support measures.

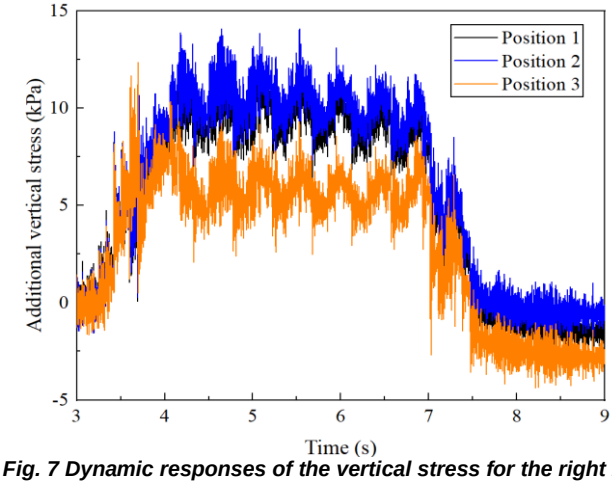

Fig. 7 Dynamic responses of the vertical stress for the right line of operating tunnel.

As can be seen from fig.7, the additional vertical stresses at monitoring point B have the same evolution law when the utility tunnel is excavated to different positions: the additional vertical stresses rise sharply when the train travels to the location of the measuring point B, and then gradually fall as the train moves away, and then fall sharply when the train leaves the measuring point. The additional vertical stresses peaks of the operating tunnel structure were 13.0 kPa, 14.0 kPa and 12.5 kPa when the utility tunnel was excavated to different locations. In addition, it is noted that the change of the additional vertical stresses at monitoring point B is most intense when the train load is fully applied to the track (about t=3.6s). The change of the additional vertical stresses is1.2kPa greater when the utility tunnel is excavated in position 3 than position 1.

In summary, although the vertical displacement and acceleration of the operating tunnel structures are not significantly affected by the excavation of utility tunnel, the additional vertical stress response is more affected by the new tunnel excavation. The impact of the lower tunnel excavation on the upper operating tunnel still needs to be fully appreciated.

3.1.3 Dynamic response characteristics of the new tunnel structure

From the above analysis, the acceleration of the operating tunnel structures under train load is less affected by the location of the utility tunnel excavation, and the acceleration amplitude of the operational tunnel structures is less than 1 m/s². Therefore, for the utility tunnel located below the operating tunnel, only the additional vertical stress response characteristics are analyzed in this section, and the additional vertical stress time curve of the utility tunnel structure is shown in fig.8.

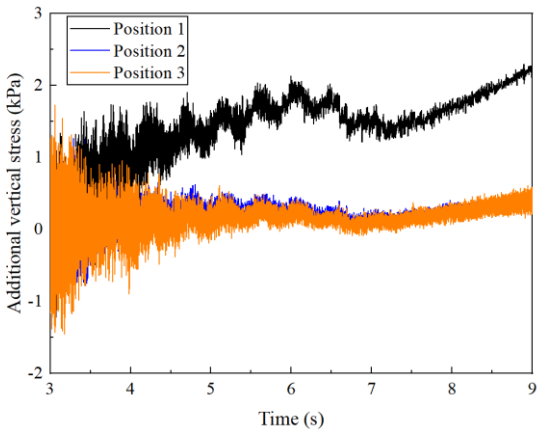

Fig. 8 Dynamic responses of the additional vertical stress for the utility tunnel.

It can be seen in fig.8, when the utility tunnel is excavated to position 1, the additional vertical stresses generated at monitoring point A_1 under train load gradually increase and eventually reach 2.5 kPa, while the additional vertical stresses generated at monitoring points A_2 and A_3 do not increase significantly and eventually stabilize at about 0.4 kPa when the utility tunnel is excavated to position 2 and position 3. It is found that the vertical additional stress generated when utility tunnel excavation in position 1 is 6.25 times higher than other positions. It shows that the dynamic response of utility tunnel structure is weakened when the utility tunnel under passed the operating tunnel.

3.2 Dynamic effects of train operating lines

From the above analysis, the dynamic response of the new tunnel is maximum when excavated to position 2. Therefore, taking the utility tunnel excavate to position 2 as an example, the dynamic response considering the interaction of the utility tunnel and the operating tunnel when the train travel in the left line, right line and both lines of the operating tunnel were compared.

3.2.1 Displacement response characteristics of old and new tunnel structures

Fig.10 shows the displacement time curves of each monitoring point when train travel in different lines.

It can be seen from fig.9 that the vertical displacement of the tunnel structures shows a trend of increasing when the train is close to the monitoring point and then gradually recovering after the train leaves. The time when the vertical displacement of different monitoring points increased sharply was different, and the vertical displacement of

monitoring point C increased sharply twice (0-1s and 4-6s) when the trains were running in both lines of the operating tunnel, which was due to monitoring point and the vibration load have different distances. At the same time, the above phenomenon also indicated that the vertical displacement of tunnel structure will generate rapidly when the train load acts on the tunnel. It can be seen in fig.10d that the closer the train load to the utility tunnel structure is, the larger its vertical displacement is. For the operating tunnel structures, the vertical displacement is larger when the train load acts on itself. The vertical displacement of the tunnel structures is larger when train load acts on two lines of the operating tunnel than others situation.

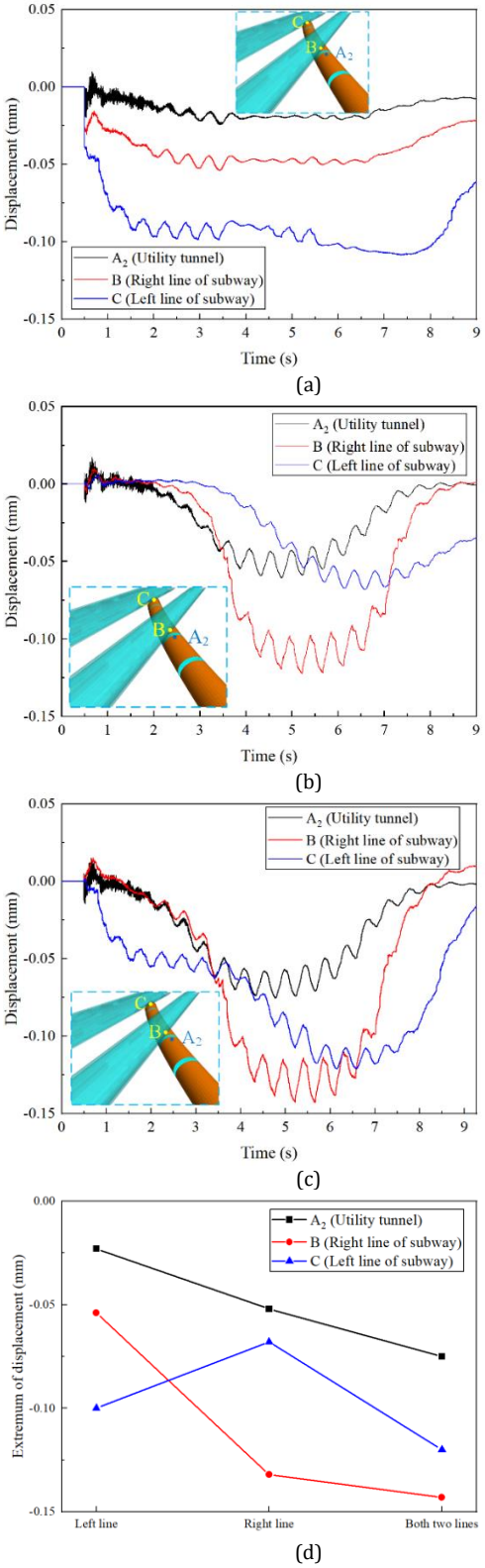

Fig. 9 Dynamic responses of the vertical displacement for the tunnels. a Train load on left line. b Train load on right line. c Train load on both lines of subway tunnels. d Extremum of displacement.

It can be seen from fig.9, the vertical displacement of each monitoring point at time of 5.6s is generally higher, so the vertical displacement cloud map of the tunnels at this time is intercepted, as shown in fig.10.

It can be seen from fig.10, when the train is running in the left line of the operating tunnel, the settlement of the left line is generally 2mm, and the settlement of the utility tunnel vault is generally 2~3mm. When the train is running in the right line of the operating tunnel, the settlement of the right line is only about 2mm behind the intersection position of the utility tunnel and operating tunnels, and the settlement of the utility tunnel vault is also 2~3mm. When the train is running in both lines of the operating tunnel, only the settlement area in the right line of the operating tunnel increases, the rest displacement distribution is similar to the situation when trains are running in the left line. In addition, when trains are running in different lines, there is an obvious difference of the right line displacement before and after the intersection of the utility tunnel and operating tunnels. This difference appears the rear of the right line when trains are running right line than in the left line. The uneven settlement is often the cause of damage to the structure and needs to be noticed.

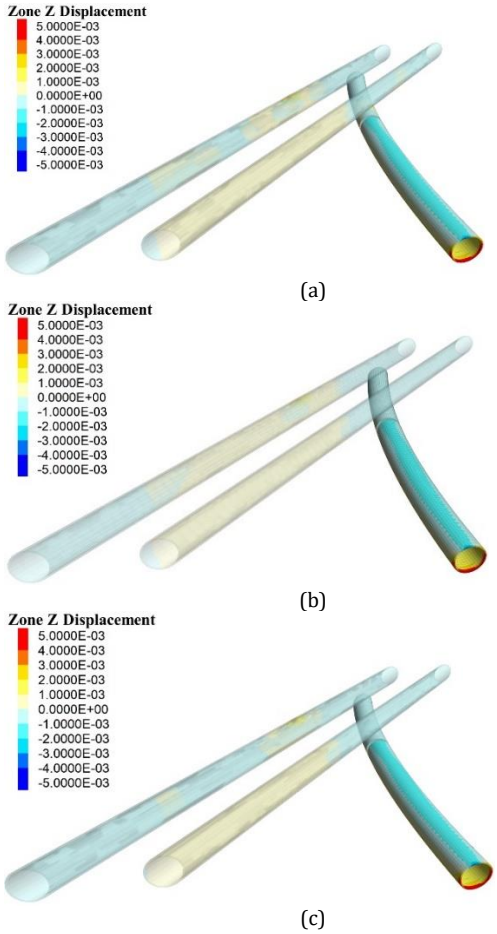

Fig. 10 Vertical displacement contour of the tunnels. a Train load on left line. b Train load on right line. c Train load on both lines of subway tunnels. (Unit: m)

3.2.2 Dynamic response characteristics of the operating tunnel structure

The acceleration time curves of measurement points B and C on the operation tunnel when the train is operating in different lines are shown in fig.11.

It can be seen from fig.11, the acceleration amplitude at the monitoring point C is lower when the train is running in the right line of the operation tunnel than others situation, and the highest value is 0.6m/s^2. When the train is running in the left line or both lines of the operation tunnel, the acceleration at monitoring point C still shows a general trend of increasing firstly and then decreasing. The vertical acceleration will rise in a short time when the train travels in the left line or in both lines of the operating tunnel, because the train travels to the monitoring point in a short time. And there are little differences of the acceleration at monitoring point C when the train travels in the left line or in both lines of the operating tunnel, its acceleration amplitude is

about 0.8m/s². For monitoring point B on the right line of the operating tunnel, when the train is running in the left line, the acceleration amplitude at monitoring point B is generally lower. When the train is running in the right line or both lines of the operating tunnel, the maximum amplitude is close to 0.97m/s². In general, the farther the vibration load from the tunnel structure is, the smaller the vibration response of the tunnel structure is. Due to the superposition of the train load, the vibration response of tunnel under the double-line load will be larger. But the dynamic response under the double-line load does not increase much, indicating that the train load has little effect on other tunnel structures after the track damping is weakened.

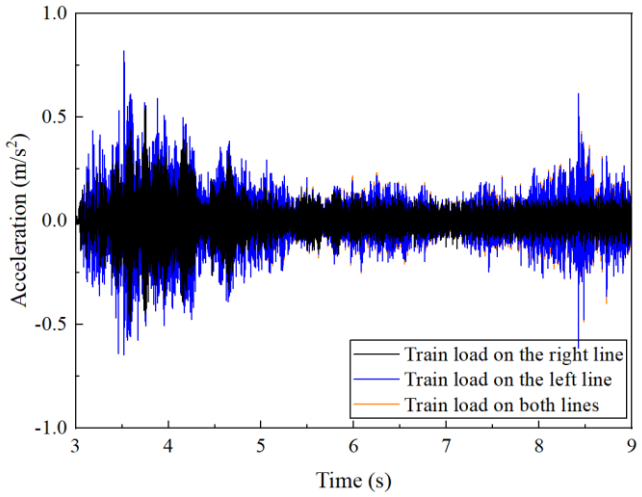

(a)

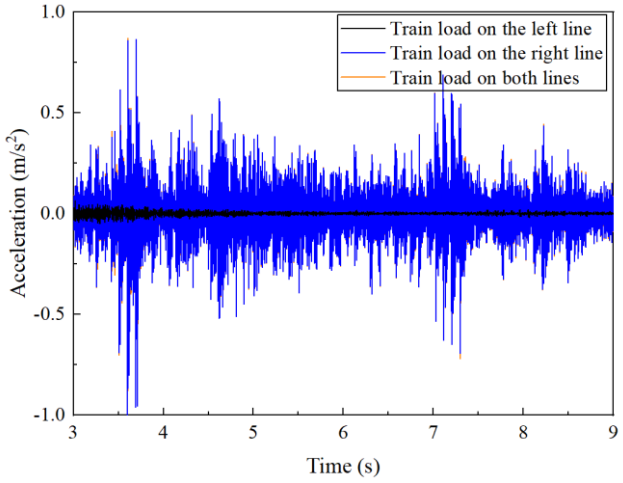

(b)

Fig. 11 Dynamic responses of the acceleration for the operating tunnel. a Monitoring point C. b Monitoring point B.

When the train operated in different lines, the time curve of vertical additional stress at monitoring points B and C on the operating tunnel is shown in fig.12.

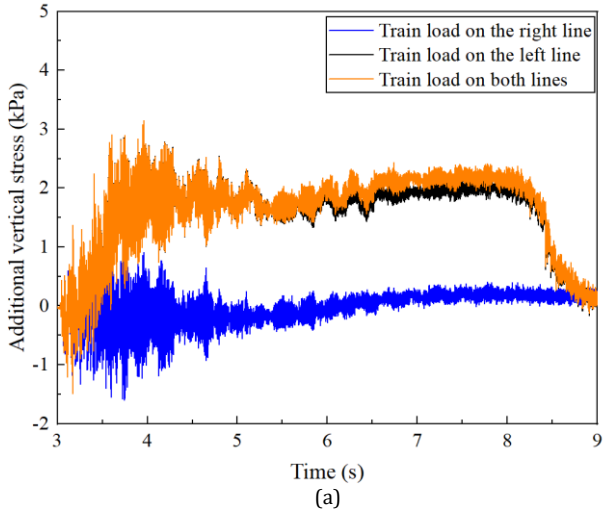

(a)

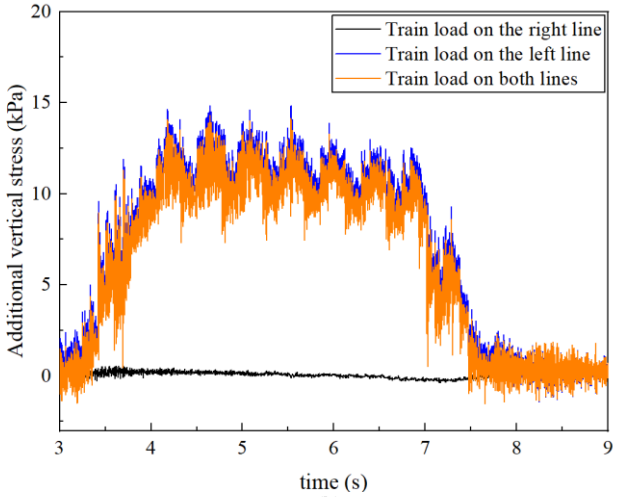

(b)

Fig. 12 Dynamic responses of the additional vertical stress for the operating tunnel. a Monitoring point C. b Monitoring point B.

It can be seen from fig.12, for monitoring point C, when the train is running in the right line of the operating tunnel, the change of the additional vertical stress at the measuring point C is little. When the train is running in the left line or both lines of the operating tunnel, the vertical additional stress at monitoring point C all show a trend of increasing firstly and then decreasing: the vertical additional stress increases when the train is close to monitoring point C, decreases when the train leaves monitoring point C, and the max additional vertical stress is around 3.0kPa. In addition, when the train load affects the monitoring point C (t=6~8s), the additional vertical stress generated by train load on both lines will exceed the additional vertical stress generated by train load on left line. For monitoring point B, when the train is running in the left line of the operating tunnel, the change of the additional vertical stress at measuring point B is little too. But the vertical additional stress at this monitoring point will rise rapidly when the train is running in the right line of both lines of the operating tunnel, with a maximum of about 14.5 kPa. The extreme value of the additional vertical stress at monitoring point B is 4.8 times higher than that at monitoring point C. The reason for this difference is that below monitoring point B is the shield shell, while below monitoring point C is the soil body and this point is far from the utility tunnel.

3.2.3 Dynamic response characteristics of the new tunnel structure

The time curve of the additional vertical stress of the utility tunnel structure under the train load is shown in Figure 13.

As shown in Figure 13, when the train is running in the left line of the operating tunnel, the vertical additional stress at monitoring point A_2 is slightly lower than it when the train is running in the right line or both lines, but the difference is less than 1 kPa. In general, the train running position has some influence on the additional vertical stress of the utility tunnel structure, but the influence is limited.

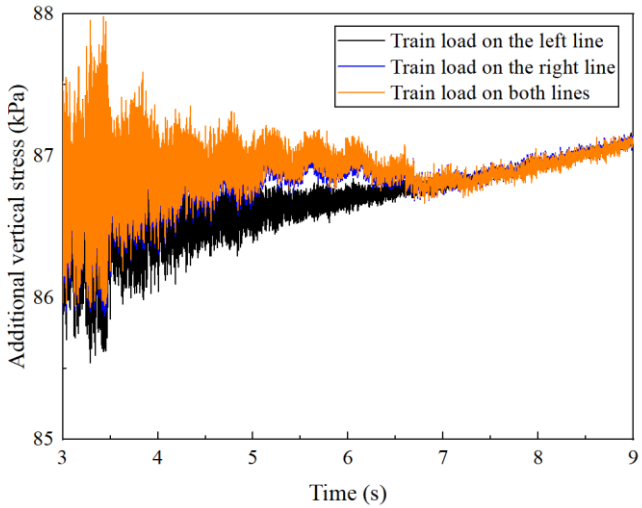

Fig. 13 Dynamic responses of the additional vertical stress for the utility tunnel under different train load.

3.3 Structural safety assessment of old and new tunnels

The safety of the tunnel structures was evaluated by taking the utility excavating to position 3 and the train running in right line of the operating tunnel as example. From the above analysis, the max settlement of the utility tunnel and operating tunnel structures is 3 mm and the extreme value of acceleration of the operating tunnel structure is 0.97 m/s^2.

The literature (Ye, 2007) considers that the deformation of the lining allowed to keep the normal operation of the tunnel is (2‰~10‰)R (R is the radius of the tunnel), and considering the high risk of this project, the deformation of 2‰R is taking in this study (taking 6mm as the lower limit of the lining deformation), The "Standard for Safety Vibration Control of Buildings" in Japan considers the structure to be at risk of damage when the vibration acceleration of the structure exceeds 1m/s^2. So, the displacement and acceleration of the tunnel structures in this project are less than the safety control index in the process of the tunnel shield under pass the operating tunnel.

Considering that the additional stress response of the tunnel structures is more intense than the displacement and acceleration response, and the tunnel structure in this study satisfies the Mohr-Coulomb yielding criterion, the yield of the tunnel structure can be determined by equation (6).

$$F = \sigma_1 - \sigma_3 - (\sigma_1 + \sigma_3)\sin\varphi - 2c\cos\varphi = 0 \quad (6)$$

Where: σ_1, σ_3 are the major and minor principal stresses respectively; φ is the angle of internal friction; c is the cohesive force.

Since the additional vertical stress of the operating tunnel structure at t=5.6s reaches a greater value of 14kPa, and the additional stress of the utility tunnel structure does not change much. Taking the utility tunnel and the operating tunnel structures in this time as example, considering c=3.18MPa and φ=50°, the yield state of the tunnels is calculated using the Flac3d embedded FISH language programming (Fig.16). As shown in fig.15, both the tunnel structures have F<0 at the overlap position, and there has no yielding occurred. This conclusion is consistent with the results that judged using displacement and acceleration index, which shows that the displacement values and dynamic response of the tunnel structures are within the allowable range during the process of the utility tunnel under construction.

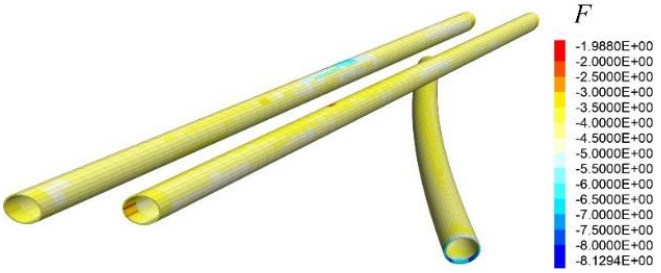

Fig. 15 Yield of tunnel structure judged by Mohr-Coulomb yielding criterion. (Unit: MPa)

4. Conclusions

Based on the utility tunnel under-passing the existing Guang-Fo subway tunnel project in the central city of Guangzhou, a 3D model of the operating tunnel-stratum-utility tunnel under construction was established. The dynamic characteristics of the operating tunnel and utility tunnel structures were studied considering the interaction between the utility tunnel and the operating tunnel during the utility tunnel construction process, and the interaction mechanism between the utility tunnel and the operating tunnel was discussed. The main conclusions show as following:

(1) When the train is operating in single line of the subway tunnel, the displacement response of both utility tunnel and operating tunnel structures shows a trend of increasing firstly and then decreasing. The extreme value of vertical displacement of all tunnel structures is slightly increased with the excavation of the utility tunnel, the increase is less than 0.01mm. The acceleration amplitude of tunnel structures is small with the excavation of the utility tunnel, the maximum change is 0.03m/s^2, but the additional vertical stress of all tunnel structures is more affected by excavation of the utility tunnel. The maximum difference of the vertical additional stress for the utility tunnel and operating tunnel structures is 1.5kPa and 2.1kPa respectively when utility tunnel excavated to different positions.

(2) The vertical displacement of the tunnel structures when the train operates in both lines is 0.05~0.1mm larger than that train operate in the single line. But the train operating in both lines has less influence on the acceleration and additional vertical stresses of the utility tunnel and the operating tunnel. The closer the utility tunnel and the operating tunnel to the train load are, its vertical displacement, acceleration and vertical additional stresses are larger during the trains operating in different lines. The operating tunnel structures which are closer to the working face of the utility tunnel have larger vertical displacement, acceleration, and additional vertical stresses.

(3) When the utility under passed the operating tunnel and the train running on the right line of the operating tunnel, there has the max settlement and acceleration of the utility tunnel and the operating structures with the value of 3mm and 0.97m/s^2 respectively. It meets the requirement of the displacement and acceleration control index. According to the Mohr-Coulomb yielding criterion, the utility tunnel and the operating tunnel structures do not yield.

References

Bo L, Peige H, Siran Z, et al. 2014. Disturbing effect of shield tunnel down-traversing nearby existing metro tunnel. 2014 7th International Conference on Intelligent Computation Technology and Automation. IEEE, 210-213.

Chen H, Yan QX, Bao R, et al. 2017. Analysis of Dynamic Response Characteristics and Damage Law for Overlapping Shield Tunnels in Small Distance Space Under Train Vibration Load. Railway Engineering, 57(12): 59-63.

Gharehdash S, Barzegar M. 2015 Numerical modeling of the dynamic behaviour of tunnel lining in shield tunneling. KSCE Journal of Civil Engineering, 19: 1626-1636.

Huang, Z, Zhang, H, Long, Z, et al. 2021. Field Test Optimization of Shield Tunnelling Parameters Undercrossing an Existing High-Speed Railway Tunnel: A Case Study. Geotechnical and Geological Engineering, 39(2), 1381–1398.

Jenkins HH, Stephenson JE, Clayton GA, et al. 1974. The effect of track and vehicle parameters on wheel/rail vertical dynamic loads. Journal of Railway Engineering Society, 3(1):2-16.

Jin D, Yuan D, Liu S, et al. 2019. Performance of Existing Subway Tunnels Undercrossed by Four Closely Spaced Shield Tunnels. Journal of Performance of Constructed Facilities, 33(1).

Li P, Du SJ, Ma XF, et al. 2014. Centrifuge investigation into the effect of new shield tunnelling on an existing underlying large-diameter tunnel. Tunnelling and Underground Space Technology, 42: 59-66.

Liang B, Cai Y. 1999. Dynamic Analysis on Subgrade of High Speed Railways in Geometric Irregular Condition. Journal of the China Railway Society, 21(2):5.

Lin ZP. 2016. Analysis on dynamic response of overlapped tunnel structure under vibration load. Journal of Railway Science and Engineering, 13(09): 1789-1795.

Liu WZ, Wang F, Luo GJ, et al. 2023. Influence of Vibration Load of Subway Elevated Train on the Stress and Deformation of Adjacent Structures. Advanced Engineering Sciences, 1-12.

Luo JY, Ding DY, Xiao XQ, et al. 2014. Prediction of deformation of adjacent existing running tunnel due to beneath shield tunneling. Applied Mechanics and Materials. Trans Tech Publications Ltd, 501: 1701-1705.

Liu N, Peng LM, Shi CH. 2016. Fatigue life prediction of tunnel base structure under the softening surrounding rock conditions. Journal of Vibration Engineering, 29(05): 936-944.

Xu LH, Ma M, Liu WN. 2020. Distribution and Evolution Characteristics of Circular Tunnel Lining Damage Due to Long-term Train Loads. Engineering Mechanics, 37(09): 144-152.

Tian LG, Cheng ZL, Hu ZQ. 2021. Numerical Investigation on Crack Propagation and Fatigue Life Estimation of Shield Lining under Train Vibration Load. Shock and Vibration.

Wang XQ, Zhang HJ, Xie WX. 2017. Experimental Study of Dynamic Cumulative Damage Model for High-speed Railway Tunnel. Tunnel Construction, 37(08): 939-945.

Shi C. 2020. Study on Macro-meso Dynamic Mechanical Behaviour of Railway Ballasted Track and Infrastructures under Vehicle loads. Southwest Jiaotong University, 2020.

Yan QX, Song LY, Chen H, et al. 2018. Dynamic Response of Segment Lining of Overlapped Shield Tunnels Under Train-Induced Vibration Loads. Arabian Journal for Science & Engineering.

Yan QX, Chen WY, Chen H, et al. 2018. Train Vibration Response Characteristics and Damage Rule of Vertically Overlapping Shield Tunnels in Close Distance Space. China Railway Science, 39(04): 78-84.

Yan QX, Liu J, Zhao SK, et al. 2010. Application of response displacement method in longitudinal seismic analysis of shield tunnel. Railway Engineering, 2010, No.437(07): 77-80.

Yang WB, Yang LL, Liang Y, et al. 2022. Study on the dynamic response characteristics of road-metro tunnels and surrounding soil under train vibration loads. Chinese Journal of Rock Mechanics and Engineering, 41(08): 1659-1670.

Ye YD. 2007. Research on Deformation and Method of Health Diagnose of Operational Subway Structures in Soft Soil. Tongji University.

Zhang J, Yan Q, Yang K, et al. 2021. Experimental modeling of adjacent parallel shield tunnels subjected to train-induced vibration loads. Proceedings of the Institution of Mechanical Engineers, Part F: Journal of Rail and Rapid Transit, 235(9): 1132-1142.